Research Square

Preprints are preliminary reports that have not undergone peer review.
They should not be considered conclusive, used to inform clinical practice,
or referenced by the media as validated information.

Synergistic Dual-Fuel-Driven Dissipative (Opto-)Electronic Crystals: Unraveling Spatiotemporal Multifunctionality Beyond Equilibrium

Pandeeswar Makam

pandeeswar.chy@itbhu.ac.in

Indian Institute of Technology (BHU) https://orcid.org/0000-0003-1114-8089

Ruchi Shukla

Indian Institute of Technology (BHU)

Rajarshi Chakraborty

Indian Institute of Technology (BHU)

Anitha Selvaraj

Vellore Institute of Technology, Chennai

Vijay Patel

Indian Institute of Technology (BHU)

Bhola Pal

Indian Institute of Technology (BHU)

Divya Korlepara

Vellore Institute of Technology, Chennai

Article

Keywords: dissipative self-assembly, (opto-)electronic crystals, spatiotemporal, adaptive materials, radical anions, out-of-equilibrium, photo-responsive

Posted Date: July 28th, 2026

DOI: https://doi.org/10.21203/rs.3.rs-10431286/v1

License: This work is licensed under a Creative Commons Attribution 4.0 International License.
Read Full License

Additional Declarations: There is **NO** Competing Interest.

Abstract

Living systems sustain complex, far-from-equilibrium structures through the continuous consumption of high-energy chemical fuels, a phenomenon known as dissipative self-assembly (DSA). While DSA has enabled the design of adaptive amorphous materials driven by a single fuel source, the construction of dissipative (opto-)electronic crystals utilizing different fuel inputs acting simultaneously remains a significant challenge. Here, we report a strategy for constructing out-of-equilibrium (opto-)electronic crystals driven by synergetic dual-fuel inputs (chemical and light). Using a bioorganic NG building block, chemical fuel consumption induces a transient condensation reaction that orchestrates successive hydration states of DSA, including colloidal particles and the formation of chiral crystals. Remarkably, the resulting dissipative crystals exhibit light-triggered transient generation of radical anions, providing an additional level of spatiotemporal regulation. Molecular dynamics simulations reveal the atomistic assembly features underlying the various states of the DSA process. Notably, this dual-fuel DSA platform endows the materials with spatiotemporally programmable multifunctionality, enabling self-erasable writing, boolean-logic-based out-of-equilibrium patterning, and dissipative (opto-)electronic device properties. These findings establish a route toward life-like programmable molecular materials with adaptive responses and autonomous information-processing capabilities, offering new opportunities for smart materials and sustainable (opto-)electronic technologies.

1. Introduction

Biological systems achieve unparalleled functional complexity by operating in a state of continuous energy flux.[1–3] In contrast to traditional synthetic materials, which often exist in a thermodynamically stable state,[4–8] living structures, such as the cytoskeletal networks composed of actin and tubulin are sustained by the constant dissipation of chemical energy, notably through ATP and GTP hydrolysis.[4, 9, 10] This non-equilibrium condition endows biological systems with essential characteristics, including temporal regulation, autonomous self-healing, and adaptive responsiveness to environmental changes.[11–13] Recently, the field of dissipative self-assembly (DSA) has emerged as an innovative approach to mimic these dynamic behaviors within synthetic molecular systems.[11, 14–16] DSA has witnessed substantial advancements in building-block design, energy-source diversification, and functionality.[17, 18] The design of building blocks has evolved from simple molecules, peptides, and amphiphiles to encompass nanoparticles and complex multi-component systems.[19–22] Moreover, energy sources have expanded beyond classical enzymatic catalysis to high-energy small-molecule reagents,[23] light in different modes,[24–28] electrical potentials,[29, 30] gases, magnetic fields, and mechanical triggers, enabling diverse kinetics, spatiotemporal control, and clean cycles.[31–33] Among these, chemical reagents and light fuels are the most frequently reported individually, reflecting their importance in driving DSA processes (Fig. 1a-b).[25] The resulting DSA structures have varied widely, ranging from fibers, micelles, and vesicles to gels, coacervates, and higher-order multicomponent structures with tunable lifetimes.[19, 31, 34] The DSA has produced several new functional behaviors that rely on transient

operating windows, including transient gels,[35] catalysis,[36] nanoreactors,[37–39] self-healable materials, [40], nanochannels,[41] nanomotors,[42] and time-gated information encryption.[43] All of these demonstrate the versatility and potential of DSA in creating materials that can respond to their environment and perform complex functions akin to those of biological systems.[18, 42, 44–46]

Despite these conceptual advances, a profound disparity remains between the intricate, multi-stimulus coordination characteristic of biological compartments and the relatively rudimentary architectures of current synthetic dissipative systems. Most established DSA platforms are constrained by their reliance on a single energy input, which predominantly yields transient, non-crystalline assemblies lacking long-range structural precision.[18, 25] Consequently, the realization of transient conducting molecular crystals —a class of materials designed to synergize the robust, long-range electronic order of organic semiconductors with the programmable temporal kinetics of non-equilibrium systems—remains a formidable and elusive challenge. Furthermore, while the field has diversified its repertoire of individual fuel sources, the orthogonal integration of multiple, distinct energy inputs dynamically regulating both structural order and electronic functionality within a single material framework is largely unprecedented. Addressing this gap requires a sophisticated molecular design that moves beyond single-stimulus responses to achieve precise, dual-gate kinetic control. Developing the capacity to spatiotemporally program the (opto-)electronic properties of self-assembled crystals through intertwined chemical and photochemical mechanisms would represent a pivotal leap forward. Such an advancement is critical not merely for mirroring biological complexity but also for realizing the next generation of intelligent materials.

To address these critical challenges, here we present a strategy for constructing dissipative (opto-)electronic molecular crystals by synergistically integrating chemical and physical (light) inputs as fuel sources. Our molecular system NG employs a naphthalenediimide (NDI) core, functionalized with glutamic acid (G) at both terminals (Fig. 1c). NDIs are intriguing π-conjugated chromophores that serve as foundational elements in supramolecular chemistry and organic electronics, due to their tuneable optoelectronic properties arising from π-stacking interactions.[47, 48] The glutamic acid modification enhances the system's solubility and responsiveness by leveraging the carboxyl group's reactivity while benefiting from its biocompatibility. This positions our NG molecular system as an ideal candidate for a fuel-driven DSA process, effectively bridging molecular design and the development of functional adaptive materials. In an aqueous environment, the bola-amphiphilic NG initially exists as a soluble monomer due to electrostatic repulsion among the carboxylate groups. The introduction of the chemical fuel, 1-ethyl-3-(3-dimethylaminopropyl) carbodiimide (EDC), promotes the dehydration of the carboxylate groups, converting them into cyclic anhydrides[49] This transformation yields uncharged, highly hydrophobic NG, which subsequently leads to colloidal aggregation to minimize exposure to the polar aqueous environment. However, the anhydrides are unstable in aqueous media, undergoing sequential hydrolysis upon depletion of the chemical fuel. First, one side of NG hydrolyzes to form an amphiphilic species, striking a delicate balance between charge and hydrophobicity that drives the lamellar self-assembly into highly ordered crystalline structures via robust π-stacking interactions.[50] This crystalline

state is inherently dissipative, as the remaining anhydride gradually hydrolyzes back to the soluble bola-amphiphilic NG, thereby completing the DSA cycle. Furthermore, under light illumination, the self-assembled crystals can be photoexcited, transitioning from a stable ground state to a higher-energy excited state, thereby generating free radicals.[51] These radical species are generated transiently and return to their ground state by dissipating energy to the environment. This mechanism facilitates the emergence of a new light-fueled DSA cycle predicated on photoexcited radicalization. The resulting DSA from both chemical and light-driven fuels enables the exploration of advanced spatiotemporal multifunctional materials. Potential applications include chemical fuel-encoded self-erasing writing, dual fuel-driven boolean-logic-based out-of-equilibrium patterning, and dissipative (opto-)electronic devices (Fig. 1d-f). Thus, our study lays the groundwork for a versatile platform, paving the way for next-generation multifuel-responsive life-like materials that possess the structural and functional precision of crystalline forms while exhibiting the dynamic plasticity characteristic of biological systems.

2. Results and discussion

2.1 Structural Evaluation of Fuel-Driven DSA of NG

The NG was synthesized using our previously established method, which involves the reaction of naphthalenediandride with L-glutamic acid in DMF under reflux, yielding a product with a favorable yield (Figure S1 & S2).[47] As shown in Fig. 2a, the NG is fully soluble in the PBS buffer at pH 6.

However, upon the introduction of EDC fuel, the initially clear NG solution immediately becomes turbid. This colloidal suspension transitions into a microcrystalline form after 10 minutes. After an additional 20 minutes, the microcrystalline, turbid solution reverts to a completely clear state, providing visual evidence of chemical fuel-driven dissipative assembly (DSA) (Fig. 2a, Movie S1). Dynamic light scattering (DLS) measurements provided quantitative insights into the temporal evolution of this fuel-driven NG assembly. The pre-fuel NG solution exhibited no assembly, characterized by a sharp band with an average hydrodynamic diameter of approximately 250 nm (Fig. 2b). Following fuel activation, self-assembly commenced immediately (t = 0 min), with a broadened band indicating an average hydrodynamic diameter of approximately 837 nm (Fig. 2c). Notably, these assemblies expanded over time, reaching a maximum average hydrodynamic diameter of 3500 nm after 10 minutes (Fig. 2d). Importantly, once the fuel was depleted after about 20 minutes, the assembly size diminished, returning to sol-state dimensions with an average hydrodynamic diameter of approximately 250 nm (Fig. 2e). This further corroborates the fuel-driven DSA of NG molecules quantitatively. To visualize the EDC-driven DSA process, we conducted optical microscopy studies. The pre-fuel NG solution was clear, showing no self-assembled structures (Fig. 2f). However, upon the addition of EDC, the solution became a suspension of colloidal particles. Under cross-polarization, these colloidal particles did not exhibit significant brightness (Fig. 2h, inset). In contrast, after standing for 10 minutes, these colloidal particles were transformed into two-dimensional (2D) assemblies. Remarkably, under polarized light, these 2D assemblies displayed bright, anisotropic birefringence, indicating well-ordered crystalline structures

(Fig. 2h). After 20 minutes, these 2D crystals dissolved back into the original clear solution, providing visual confirmation of EDC-driven DSA of NG (Fig. 2i, Movie S2). In alignment with the optical microscopy observations, high-resolution scanning electron microscopy (HR-SEM) images revealed the formation of square-shaped 2D microstructures with lateral dimensions of 100 μm, observed 10 min after the addition of EDC to the NG solution (Fig. 2j). Notably, after 20 min of EDC addition, no significant structures were observed, indicating EDC-driven DSA. High-resolution transmission electron microscopy (HR-TEM) analyses revealed a thin, nanolayered hierarchy within the 2D microcrystals (Fig. 2k). Additionally, powder X-ray diffraction (PXRD) analyses at each state of NG assembly following EDC addition were recorded and compared (Fig. 2l). At both 0 minutes and 20 minutes post-EDC introduction, the PXRD patterns indicated an amorphous nature. In contrast, the sample at 10 minutes post-EDC addition exhibited a sharp, intense PXRD pattern corresponding to a square-shaped 2D assembly, indicating well-ordered crystalline organization of the molecules. Circular dichroism (CD) spectral studies have provided valuable insights into the supramolecular organization of NG upon the addition of EDC, as observed at 0, 10, and 20 minutes (Fig. 2m). The initial NG solution exhibited a flat CD signal, indicating the absence of chiral assemblies. However, upon addition of EDC at 0 minutes, strong induced Cotton effects emerged in the 320–430 nm wavelength range, attributed to the characteristic π–π* transitions of NDI chromophores aligned along their long axes. After 10 minutes following EDC addition, these bands intensified into a prominent negative bisignate couplet centered at 394 nm, signifying a left-handed, M-type helical arrangement of adjacent NDI long-axis transition dipoles within the 2D crystal structures. Notably, after 20 minutes, the induced CD signals diminished to a flat baseline, returning to the initial state of molecularly dissolved components without assembly. Overall, this CD study effectively demonstrates the transient chiroptical switching assembly properties of NG driven by the fuel EDC, highlighting the system's time-gated dynamic chiral self-assembly behavior.

2.2 Spectroscopic Characterization of NG Fuel-Driven DSA Process

The fuel-driven DSA process in NG was further characterized using UV-visible absorption studies. As shown in Fig. 3a, the NG solution undergoes a reversible visual transition from clear to turbid upon the addition of EDC, then returns to clear after the fuel is consumed (Movie S1). The UV–visible absorption spectra of NG and EDC-fueled NG were analyzed at distinct time intervals (t = 0, 10, and 20 minutes after EDC addition), providing crucial insights into the fuel-driven transient self-assembly process (Fig. 3b). In the clear NG solution, sharp, well-defined absorption bands appeared in the range of 300–400 nm (band I), which are associated with characteristic π–π* transitions along the long axis (z-axis) of the NDI chromophore, indicating a molecularly dissolved state.[52] Notably, the EDC-fueled NG solution at 0 minutes exhibited a new broad band in the higher wavelength region (410–700 nm) attributed to scattering from the turbid solution. After 10 minutes following EDC addition, the NG solution displayed a less intense and broader band I, alongside a non-zero baseline, suggesting significant intermolecular π–π stacking among the NDI chromophores, leading to the formation of a 2D microcrystal suspension. Remarkably, after 20 minutes of EDC fueling, the NG solution again presented a well-defined band I, akin to the pre-fueled state, indicating the dissipative nature of the EDC-driven self-assembly process. This

phenomenon was further corroborated by the NG aggregation percentage (α%) profile observed after multiple EDC addition cycles to NG (Fig. 3c). Each EDC addition led to immediate maximum aggregation (at 0 minutes), followed by a gradual return to the molecularly dissolved state over 20 minutes. Moreover, this fuel-driven dissipative self-assembly exhibited reversible behavior even after four cycles of operation. These findings confirm that NG initially exists in a clear, molecularly dissolved state, which transitions to two distinct self-assembled states upon the addition of EDC fuel: a colloidal state at 0 minutes and 2D microcrystals at 10 minutes. After standing for 20 minutes, the entire system reverts to the molecularly dissolved state, highlighting the transient nature of this fuel-driven NG self-assembly process.

The ability to achieve a stable, repeatable, and fully reversible transition between molecularly dissolved states and self-assembled states is critical for the functionality of the DSA process. In this study, we systematically optimized key parameters, including the chemical fuel (EDC), precursor (NG), and solution pH, that govern the DSA process. We monitored the time-dependent relative percentage of aggregation (α, %) across three distinct states: colloidal assembly (t = 0 min), 2D crystalline assembly (t = 10 min), and reversion to the molecularly dissolved state (t = 20 min). Kinetic studies revealed that EDC concentration plays a crucial role in activating the NG through the three DSA states over a 20-min duration. Specifically, a concentration of 20 mM EDC was identified as optimal for achieving three complete states of DSA. Concentrations below this threshold did not induce significant assembly, while concentrations exceeding 20 mM resulted in longer-lived self-assembled states, hindering the system's ability to revert to the dissolved state (Fig. 3d & S2). Meanwhile, kinetic studies on varying NG concentrations (2–10 mM) demonstrated time-gated self-assembly with diverse lifetimes (Fig. 3e & S2). The optimal NG concentration of 10 mM produced the highest degree of self-assembly at both 0 min and 10 min, while ensuring complete reversibility to the molecularly dissolved state over the 20 min period. These findings underscore the critical role of chemical fuel (EDC) and precursor (NG) concentrations in modulating the lifetime of self-assembly during different states of the DSA process. Additionally, we investigated the influence of solution pH on activation kinetics, revealing that the entire DSA cycle could be effectively observed under acidic conditions (pH ≤ 7). Notably, pH 6 emerged as the optimal condition, achieving a well-balanced distribution among the three DSA states. Conversely, under basic conditions (pH > 7), we observed minimal or no DSA due to significant inhibition of EDC activation (Fig. 3f & S2). Through this comprehensive optimization study, we identified a synergistic parameter set comprising 20 mM EDC, 10 mM NG, and pH 6. This combination facilitated robust, fully reversible transient self-assembly and established optimal conditions for subsequent time-gated characterization studies, providing a reliable platform for exploring NG's DSA processes.

Next, we investigated the NG’s light-fueled DSA properties. Upon exposure to 365 nm UV light (intensity 1 $W.m^{-2}$) for 15 seconds, the initially self-assembled, white, turbid solution of NG turns deep brown. When the irradiation ceases, the solution quickly reverts to its original white, turbid appearance within 5 minutes (Fig. 3g). The UV-visible absorption spectra obtained following light stimulation reveal distinctive bimodal band I absorption peaks of NDI. Notably, these spectra exhibit significant broadening and a 5 nm hypsochromic shift compared to spectra recorded before and after EDC-fueled NG.

Additionally, two new weak, broad absorption bands appeared at 450 nm and 550 nm, suggesting the formation of NDI radical anions.[51] (Fig. 3h). Upon repeated cycles of light activation and deactivation, the system exhibits reversible spectral absorption at 450 nm, accompanied by corresponding color changes in the solution over 4 cycles, each lasting 5 minutes (Fig. 3i). These findings further substantiate that the NG undergoes spontaneous DSA driven by the synergistic dual effects of chemical and light fuels.

2.3 Characterizing NG Fuel-Driven Chemical Changes in DSA Process

To elucidate the molecular-level chemical transformations of NG during the various states of the EDC-fuel-driven DSA process, a series of spectroscopic studies was conducted. The zeta potential values of the NG solution were recorded both before and after EDC addition at various time intervals (0, 10, and 20 minutes) (Fig. 4a). Initially, the NG solution exhibited a zeta potential of -10.4 mV, indicating the presence of glutamate terminal groups at both ends of the NG molecules. Importantly, upon the immediate addition of EDC (at 0 minutes), the zeta potential decreased to 0 mV, signifying the formation of fuel-driven neutral anhydrides on both sides of the NG molecule. After 10 minutes, the zeta potential had risen to -5.4 mV, which suggests the presence of one glutamate group and one anhydride. By the 20-minute mark, the zeta potential increased further to -9.0 mV, approaching the initial value of the pre-fueled NG solution. This observation implies that the anhydride is hydrolyzed.

back into carboxylates on both sides of the NG molecule. To substantiate these findings, Fourier-transform infrared (FT-IR) spectroscopy was utilized. Samples were acidified to pH 4.5 to halt the DSA process at each state and to facilitate monitoring of carboxylic acid groups at both ends of the NG. The FT-IR spectrum of the pre-fueled NG solution revealed characteristic O-H stretching frequencies associated with carboxylic acids, spanning the range of 3535–3044 cm^{-1}. Remarkably, immediately following the addition of EDC (at 0 minutes), the O-H stretching frequencies vanished, coinciding with the emergence of distinct bands indicative of anhydride carbonyl (C = O) groups within the region of 1846–1650 cm^{-1}.[53] After 10 minutes, the anhydride carbonyl bands began to broaden, accompanied by a simultaneous re-emergence of the carboxylic acid O-H stretching bands. By 20 minutes, the intensity of the anhydride carbonyl bands had diminished significantly, while the intensity of the carboxylic acid O-H stretching band had increased, indicating a transition back to pre-fueled NG state (Fig. 4b). Time-dependent ^{1}H-NMR studies revealed a singlet aromatic NDI chemical shift at 8.66 ppm prior to the introduction of EDC, attributable to the symmetric glutamic acid environment on both sides of the NG (Fig. 4c). Upon addition of EDC, the signal split into two unequal sharp peaks, indicating a chemical transformation. After 10 minutes, the signals began to broaden and reached equal intensities, indicating a transition to an asymmetric chemical environment on either side of NG, thereby inducing aromatic stacking. Notably, after 20 minutes, the two signals coalesced into a single peak resembling the original singlet of the pre-fueled NG. Collectively, these spectral investigations demonstrate that the pre-fueled NG exists as glutamate anions on both ends, maintained in a molecularly dissolved state due to electrostatic repulsion. The immediate introduction of EDC converts the anionic glutamate groups into

neutral anhydrides, thereby significantly enhancing the hydrophobicity of NG and enabling random colloidal organization. However, anhydrides are inherently unstable in aqueous environments; therefore, at the 10-minute mark, one side of the anhydride hydrolyses back to glutamate, transitioning the NG into an amphiphilic state conducive to highly ordered crystalline self-assembly. Further analysis at the 20-min mark indicates that the remaining anhydride also hydrolyzes back to glutamate on both sides of the NG, thereby reverting the NG to an anionic form and dissolving the crystals into a molecularly dissolved state, completing the DSA cycle (Fig. 4d).

2.4 Insights from Molecular Dynamics (MD) Simulations on the EDC-Driven DSA in NG

Following the confirmation of EDC-driven molecular structures of NG at various states of DSA, we conducted molecular dynamics (MD) simulations to explore the complex atomistic behaviors associated with self-assembly during these distinct states. We selected three representative molecular structures for analysis: the pre-fueled NG, which characterizes the molecularly dissolved state; the 0-min post-fueled NG, which forms turbid colloids immediately after EDC treatment; and the 10-min post-fueled NG, which displays crystalline characteristics approximately 10 min after EDC treatment (Fig. 5a-c & S4). Each of these molecular structures underwent 850 ns of MD simulations in an aqueous environment, providing detailed insights into their self-assembly behavior. Time-resolved snapshots from our simulations revealed significant differences in assembly mechanisms across the three DSA states. Notably, the pre-fueled NG molecules remained monomeric throughout the simulation, showing no significant tendency to self-assemble (Fig. 5d). This observation is consistent with experimental results indicating a clear, homogeneous NG solution. Conversely, the 0-minute post-fueled NG system initially appeared as a monomeric ensemble at 0 ns; however, cluster formation emerged around 300 ns and persisted throughout the simulation (Fig. 5e). These transient clusters exhibited a relatively disordered structure, indicative of an intermediate colloidal state. At the 10-min post-fueling mark, NG molecules predominantly formed dimers at the simulation's onset, which subsequently evolved into well-ordered, linear π-stacked assemblies characterized by supramolecular polymerization. By the conclusion of the 850 ns simulation, the longest observed polymer consisted of four stacked units, suggesting a successful transition towards greater structural organization (Fig. 5f). Temporal evolution further supported this behavior, revealing a progressive increase in supramolecular polymer length.

over time (Fig. 5g & S6). The pre-fueled NG maintained a consistent polymer length of one throughout the simulation, reinforcing its status as a molecularly dissolved entity. In the case of the 0-min post-fueled NG, we observed dynamic oligomerization, evidenced by short-lived trimers that ultimately dissociated and reassociated into cluster-like structures. In contrast, the 10-minute post-fueled NG exhibited the onset of supramolecular polymerization at approximately 400 ns, followed by sustained chain growth, highlighting enhanced assembly efficiency and structural integrity in this state.[54] To further investigate the strength of aromatic π-stacking interactions, we analyzed the center-of-mass (COM) distances between neighboring aromatic NDI cores (Figure S5). The pre-fueled NG system demonstrated a broad COM–COM distance distribution extending up to 4.0 Å, indicating minimal

aromatic stacking interactions and a highly disordered molecularly dissolved state. In comparison, the post-fueled 0-min NG showed a slightly narrower distribution, peaking at 3.8 Å, which aligns with the characteristics of partially ordered colloids. In sharp contrast, the 10-minute post-fueled NG exhibited a significantly narrower COM–COM distance distribution, confined to approximately 3.6 Å, indicative of compact, ordered molecular π-stacks that correspond with the experimentally observed crystalline structures (Fig. 5h & S7). Moreover, an analysis of the twist angles between adjacent aromatic units revealed distinct conformational characteristics across the three states. Both the pre-fueled and post-fueled 0-min NG systems exhibited a broad twist-angle distribution from 60° to 120°, indicating substantial conformational flexibility and the absence of a well-defined stacking geometry. Conversely, the 10-min post-fueled NG maintained a well-defined twist angle of approximately 90°, a configuration known to optimize π–π stacking interactions and support long-range molecular organization (Fig. 5i & S7). In summary, the insights gained from these MD simulation studies not only validate the experimentally observed DSA states of NG but also clarify the intricate mechanisms governing the transition from molecular dissolution to colloids, culminating in enhanced crystalline order. This comprehensive understanding of self-assembly processes in NG carries significant implications for the development and optimization of NG-based systems across various applications.

2.5 Synergetic Dual Fuel-Driven Spatiotemporal Multifunctionality Beyond Equilibrium

Unlike conventional self-assembly methods, which yield static architectures, DSA offers a novel strategy for creating spatiotemporal functionalities that evolve. A primary advantage of DSA systems is their capacity to induce physical changes that can be programmatically controlled and erased, enabling adaptive responses to environmental stimuli. This characteristic holds significant promise for applications in volatile data storage and smart materials, where transient behaviors are critical for efficient data management and processing. In our initial demonstration of DSA, we observed color transitions from a colorless solution to an EDC-driven white, turbid colloidal and microcrystalline suspension that eventually turned deep brown under light illumination. Building upon these observations, our goal was to convert these unique phenomena into spatiotemporal writing and patterns that exhibit predetermined self-erasure over time. We successfully generated transient white, turbid, microcrystalline writing pattern in a 96-well plate filled with a colorless NG solution. By selectively applying EDC with a micropipette to specific areas of the well plate, we created an “IIT” writing pattern, transforming the targeted regions into a white, turbid microcrystalline pattern that subsequently self-erased. This writing pattern could be rewritten after each cycle by reapplying EDC, thus establishing a method for spatiotemporal transient patterning that ensures time-gated erasure (Fig. 6a).[13] Furthermore, we observed that EDC-driven NG turbid suspension briefly turns deep brown upon exposure to light. Leveraging these findings, we developed a synergistic dual-fuel system wherein both EDC and light drive the formation of transient patterns. Upon introducing EDC into the NG solution, the initially colorless mixture became a turbid, white, microcrystalline suspension (Fig. 6b). We then illuminated this mixture with UV light for 20 seconds through a star-shaped photomask. The area exposed to UV light quickly developed a deep-brown star pattern due to the photoinduced generation of the NDI radical anion. Once

the light source was removed, the pattern exhibited high transience, self-erasing over time back to a white turbid microcrystal state before ultimately reverting to a colorless NG solution. Remarkably, this patterning and erasing process can be repeated. Utilizing the distinct colorimetric properties of our dual-fueled NG system, we also developed a transient logic gate. In this configuration, specific combinations of input fuels yield predefined output patterns. These fuel-driven transient logic gates are innovative, dynamic computing elements that operate outside equilibrium, enabling temporary information processing and adaptive material responses akin to those observed in biological systems. In this framework, EDC and light function as input signals, while the resultant deep brown patterns serve as output signals. Specifically, the interaction of these input fuels generates NG radical anions, resulting in a deep brown star pattern, indicative of an output value of 1. The accompanying truth table illustrates the functionality of an “AND” logic gate, indicating that the output is 1 only when both EDC and light are present; the absence of either input results in zero output (Output = 0), effectively fulfilling the conditions of an AND gate operation (Fig. 6c). The implications of these findings are profound, with the potential to revolutionize the fields of smart materials and dynamic computing. The integration of self-erasing patterns and adaptive logic gates marks a significant advancement in materials science, paving the way for the development of systems capable of responsive behavior, temporary data storage, and information processing with minimal energy consumption.

Moreover, due to electron delocalization within the anticipated close-range aromatic stacking of NG molecules in the observed DSA microcrystals, we postulated that the dynamic processes of assembly and disassembly would enable temporal control over electrical conduction. As illustrated in Fig. 6d, the device configuration, comprising ITO electrodes patterned on a glass substrate, was used to measure time-dependent current variations with and without EDC fuel. In the pre-fuel NG homogeneous solution state, the device exhibits minimal electrical current (~ 1×10^{-8} A; Fig. 6e), consistent with the molecularly dissolved state, in which there is no interconnected molecular network. Upon EDC addition, the homogeneous, clear solution rapidly transitions to a turbid colloidal suspension, resulting in a sharp increase in the device current to ~ 2.5×10^{-7} within ~ 10 s. Continued self-assembly into the microcrystalline state after approximately 100 s resulted in a further sharp increase in device current (~ 1×10^{-6} A), attributed to highly ordered crystalline molecular packing and efficient aromatic π–π stacking interactions among the NDI cores, thereby facilitating effective electron-hopping conduction. This elevated current is maintained transiently, reflecting effective charge delocalization across the self-assembled 2D microcrystals. As the chemical fuel is depleted and the hydrolysis reaction progresses, the 2D microcrystals disassemble back into the homogeneous, clear solution, accompanied by a return of the current to its baseline value (~ 1×10^{-8} A), clearly demonstrating the DSA-induced transient electrical-conducting characteristics of the device. Next, the impact of light-driven transient radical generation on electrical conduction was evaluated in the microcrystalline state using a similar device configuration illustrated in Fig. 6d. In the absence of light, the maximum current recorded for the EDC-fueled microcrystalline state was approximately 1×10^{-6} A. Notably, upon illumination with UV light (1 W m^{-2}) during current-voltage (I-V) assessments, we observed a 150-fold increase in current, rising to approximately 1.5×10^{-4} A (as shown in Fig. 6f). This photoirradiation of the NG microcrystals facilitates

the generation of radical-anion charge carriers, which effectively lowers the energy gap and promotes enhanced photocurrent relative to the neutral assembly.[55] It is crucial to highlight that the light-induced NG radical anions are transient species, with their concentration being dependent on continuous exposure to UV light. Consequently, once the illumination is ceased, the current reverts to its baseline level. Furthermore, this light-triggered modulation of electrical conduction was found to be reproducible across multiple ON–OFF cycles, as depicted in Fig. 6g, which presents the current-time (I-T) measurements at 1 V. The shaded regions in the figure denote the intervals under illumination (blue) and in the dark (black), further demonstrating the robustness of optoelectronic switching behavior. This significant role of light-induced radical generation in enhancing the electrical properties of NG microcrystals paves the way for advances in dissipative optoelectronic materials.

3. Conclusion

In summary, this research represents a significant advancement in the field of DSA, introducing a new dual-fuel-driven approach to constructing optoelectronic crystals that operate beyond conventional thermodynamic equilibrium. By leveraging a bioorganic NG building block activated by both chemical and light fuels, we have achieved remarkable control over the DSA process, enabling intricate spatiotemporal manipulation of the assembly dynamics. The chemical fuel, EDC, plays a critical role in transitioning the molecularly dissolved NG into a higher-energy anhydride-active building block, which subsequently undergoes a sequence of hydrolysis reactions. This process yields thermodynamically out-of-equilibrium colloids and chiral crystals, which ultimately return to a molecularly dissolved state, completing the DSA cycle. The transient generation of radical anions upon light activation not only enhances the functionality of the resulting dissipative materials but also establishes a pioneering foundation for the development of programmable materials that can adapt in a manner akin to biological systems. Through comprehensive spectroscopic and microscopic analyses, we have elucidated the mechanisms governing the transient structural evolution at each state of the DSA process. Complementary MD simulations have provided crucial insights into the atomic-level structure-assembly characteristics, further corroborating our experimental observations. This dual-fuel DSA platform significantly enriches the functionality of dissipative materials, enabling applications such as self-erasable information writing, precise spatiotemporal boolean gate patterning, and enhanced integration of (opto-)electronic properties. By harnessing multiple fuel sources, we unlock new potential for DSA, a transformative technique that emulates lifelike behaviors and revolutionizes the field of synthetic materials. Our findings contribute to the burgeoning domains of bioelectronics and sustainable (opto-)electronic technologies, envisioning materials that respond dynamically to environmental stimuli while demonstrating autonomous information-processing capabilities. Moving forward, our efforts will focus on optimizing production processes for practical applications, thereby expanding the applicability of these advanced materials in innovative fields such as smart electronics, sensors, and energy harvesting. Overall, this research marks a pivotal stride in utilizing the principles of DSA to create multifunctional materials, heralding a new era of transformative applications in materials science and bioengineering.

Declarations

Conflicts of Interest

The authors declare no conflicts of interest.

Acknowledgments

P.M. acknowledges the support of ICMR, India (IIRPSG 2024-01-03827) and IIT (BHU) (IIT(BHU)/R&D/2025-26/ CPCG-01/725). D.B.K. and A.S. gratefully acknowledge access to the Crystal High Performance Computing Cluster (CHPCC) of the Department of Physics, School of Advanced Sciences, VIT Chennai Campus. R.S. and P.M. thanks to the HPC facility at IIT (BHU). R.S. thanks DST-INSPIRE research fellowship (IF210343). R.C. thanks IIT (BHU) for the SRF fellowship. V.K.P. thanks the UGC-India research fellowship. R.S, R.C., V.K.P., B.N.P., and P.M. acknowledge the IIT (BHU) Central Instrumentation Facility.

References

1. Vale RD, Milligan RA (2000) The way things move: Looking under the hood of molecular motor proteins. Sci (80-) 288:88
2. Pantaloni D, Le Clainche C, Carlier M (2001) Mechanism of Actin-Based Motility. Sci (80-) 292:1502–1506
3. Fletcher DA, Mullins RD (2010) Cell mechanics and the cytoskeleton. Nature 463:485–492
4. Mattia E, Otto S (2015) Supramolecular systems chemistry. Nat Nanotechnol 10:111–119
5. Vishwakarma S, Tiwari OS, Shukla R, Gazit E, Makam P (2024) Amyloid inspired single amino acid (phenylalanine)-based supramolecular functional assemblies: from disease to device applications. Chem Soc Rev 54:465–483
6. Tao K, Makam P, Aizen R, Gazit E (2017) Self-assembling peptide semiconductors. Sci (80-). 358
7. Aida T, Meijer EW, Stupp SI (2012) Functional Supramolecular Polymers. Sci (80-) 335:813–817
8. Makam P, Gazit E (2018) Minimalistic peptide supramolecular co-assembly: Expanding the conformational space for nanotechnology. Chem Soc Rev 47:3406–3420
9. Valiron O, Caudron N, Job D (2001) Microtubule dynamics. Cell Mol Life Sci 58:2069–2084
10. Singh A, Parvin P, Saha B, Das D (2024) Non-equilibrium self-assembly for living matter-like properties. Nat Rev Chem 8:723–740
11. van Rossum SAP, Tena-Solsona M, van Esch JH, Eelkema R, Boekhoven J (2017) Dissipative out-of-equilibrium assembly of man-made supramolecular materials. Chem Soc Rev 46:5519–5535
12. Grzybowski BA, Fitzner K, Paczesny J, Granick S (2017) From dynamic self-assembly to networked chemical systems. Chem Soc Rev 46:5647–5678

13. Tena-Solsona M et al (2017) Non-equilibrium dissipative supramolecular materials with a tunable lifetime. Nat Commun 8:1–8
14. Van Esch JH, Klajn R, Otto S (2017) Chemical systems out of equilibrium. Chem Soc Rev 46:5474–5475
15. Boekhoven J, Hendriksen WE, Koper GJM, Eelkema R, van Esch JH (2015) Transient assembly of active materials fueled by a chemical reaction. Sci (80-) 349:1075–1079
16. De S, Klajn R (2018) Dissipative Self-Assembly Driven by the Consumption of Chemical Fuels. Adv Mater 30:e1706750
17. Hou X et al (2023) Supramolecular dissipative self-assembly systems: Approaches and applications. Responsive Mater 1
18. Sharko A, Livitz D, De Piccoli S, Bishop KJM, Hermans TM (2022) Insights into Chemically Fueled Supramolecular Polymers. Chem Rev 122:11759–11777
19. della Sala F, Neri S, Maiti S, Chen JLY, Prins LJ (2017) Transient self-assembly of molecular nanostructures driven by chemical fuels. Curr Opin Biotechnol 46:27–33
20. Xu F et al (2022) Dynamic Control of a Multistate Chiral Supramolecular Polymer in Water. J Am Chem Soc 144:6019–6027
21. Qin S, Geng Y, Discher DE, Yang S (2006) Temperature-controlled assembly and release from polymer vesicles of poly(ethylene oxide)-block-poly(N-isopropylacrylamide). Adv Mater 18:2905–2909
22. Ravarino P et al (2023) Controlled Annealing in Adaptive Multicomponent Gels. Angew Chem Int Ed Engl 62:e202215813
23. Borsley S, Leigh DA, Roberts BM (2022) W. Chemical fuels for molecular machinery. Nat Chem 14:728–738
24. Kim J et al (2015) Induction and control of supramolecular chirality by light in self-assembled helical nanostructures. Nat Commun 6:6959
25. Weißenfels M, Gemen J, Klajn R (2021) Dissipative Self-Assembly: Fueling with Chemicals versus Light. Chem 7:23–37
26. Wang X et al (2015) Reversibly Switching Bilayer Permeability and Release Modules of Photochromic Polymersomes Stabilized by Cooperative Noncovalent Interactions. J Am Chem Soc 137:15262–15275
27. Faramarzi V et al (2012) Light-triggered self-construction of supramolecular organic nanowires as metallic interconnects. Nat Chem 4:485–490
28. Chen C, Valera JS, Adachi TBM, Hermans TM (2023) Efficient Photoredox Cycles to Control Perylenediimide Self-Assembly**. Chem - Eur J 29:e202202849
29. Selmani S et al (2022) Electrically Fueled Active Supramolecular Materials. J Am Chem Soc 144:7844–7851

30. Chen C, Guan Z (2023) Precise Control of Dissipative Self-assembly by Light and Electricity. Chem - Eur J 29:e202300347
31. Ragazzon G, Prins LJ (2018) Energy consumption in chemical fuel-driven self-assembly. Nat Nanotechnol 13:882–889
32. Leira-Iglesias J, Tassoni A, Adachi T, Stich M, Hermans TM (2018) Oscillations, travelling fronts and patterns in a supramolecular system. Nat Nanotechnol 13:1021–1027
33. Xue P et al (2021) Near-Infrared Light-Driven Shape-Morphing of Programmable Anisotropic Hydrogels Enabled by MXene Nanosheets. Angew Chemie - Int Ed 60:3390–3396
34. Arango-Restrepo A, Barragán D, Rubi JM (2019) Self-assembling outside equilibrium: Emergence of structures mediated by dissipation. Phys Chem Chem Phys 21:17475–17493
35. Tang J, Cheng Y, Ding M, Wang C (2023) Bio-Inspired Far-From-Equilibrium Hydrogels: Design Principles and Applications. *Chempluschem* 88
36. Cui S, Zhang J, Fu J, Deng Z, Liu S (2026) Harnessing Dynamic Self-Assembly to Accelerate Chemical Reactions. Small Struct 7
37. Hirst AR et al (2010) Biocatalytic induction of supramolecular order. Nat Chem 2:1089–1094
38. Maiti S, Fortunati I, Ferrante C, Scrimin P, Prins LJ (2016) Dissipative self-assembly of vesicular nanoreactors. Nat Chem 8:725–731
39. Harris R, Berman N, Lampel A (2025) Coacervates as enzymatic microreactors. Chem Soc Rev 54:4183–4199
40. Wei T, Tang Z, Yu Q, Chen H (2017) Smart Antibacterial Surfaces with Switchable Bacteria-Killing and Bacteria-Releasing Capabilities. ACS Appl Mater Interfaces 9:37511–37523
41. Grötsch RK et al (2019) Pathway Dependence in the Fuel-Driven Dissipative Self-Assembly of Nanoparticles. J Am Chem Soc 141:9872–9878
42. Hess H, Ross JL (2017) Non-equilibrium assembly of microtubules: From molecules to autonomous chemical robots. Chem Soc Rev 46:5570–5587
43. Wang Q, Qi Z, Chen M, Qu DH (2021) Out-of-equilibrium supramolecular self-assembling systems driven by chemical fuel. Aggregate 2
44. Merindol R, Walther A (2017) Materials learning from life: Concepts for active, adaptive and autonomous molecular systems. Chem Soc Rev 46:5588–5619
45. Biagini C et al (2019) Dissipative Catalysis with a Molecular Machine. Angew Chemie - Int Ed 58:9876–9880
46. Shukla R et al (2025) Bioinspired Out-of-Equilibrium Conductive Hydrogels: Unlocking Fuel and Light-Responsive Transient Conducting Properties. ACS Nano 19:42319–42330
47. Pandeeswar M, Khare H, Ramakumar S, Govindaraju T (2014) Biomimetic molecular organization of naphthalene diimide in the solid state: Tunable (chiro-) optical, viscoelastic and nanoscale properties. RSC Adv 4:20154–20163

48. Pandeeswar M, Senanayak SP, Narayan KS, Govindaraju T (2016) Multi-Stimuli-Responsive Charge-Transfer Hydrogel for Room-Temperature Organic Ferroelectric Thin-Film Devices. J Am Chem Soc 138:8259–8268
49. Schnitter F et al (2021) Synthesis and characterization of chemically fueled supramolecular materials driven by carbodiimide-based fuels. Nat Protoc 16:3901–3932
50. Pandeeswar M, Khare H, Ramakumar S, Govindaraju T (2015) Crystallographic insight-guided nanoarchitectonics and conductivity modulation of an n-type organic semiconductor through peptide conjugation. Chem Commun 51:8315–8318
51. Saha M, Bandyopadhyay S (2021) Stimuli Responsive Stable Radical Anion for Conductance Switching. J Phys Chem C 125:6427–6432
52. Shao H et al (2010) Amphiphilic Self-Assembly of an n-Type Nanotube. Angew Chemie 122:7854–7857
53. Kariyawasam LS, Hartley CS (2017) Dissipative Assembly of Aqueous Carboxylic Acid Anhydrides Fueled by Carbodiimides. J Am Chem Soc 139:11949–11955
54. Mishra A et al (2018) Biomimetic temporal self-assembly via fuel-driven controlled supramolecular polymerization. Nat Commun 9:1–9
55. Bakulin AA et al (2012) The Role of Driving Energy and Delocalized States for Charge Separation in Organic Semiconductors. Sci (80-) 335:1340–1344

Figures

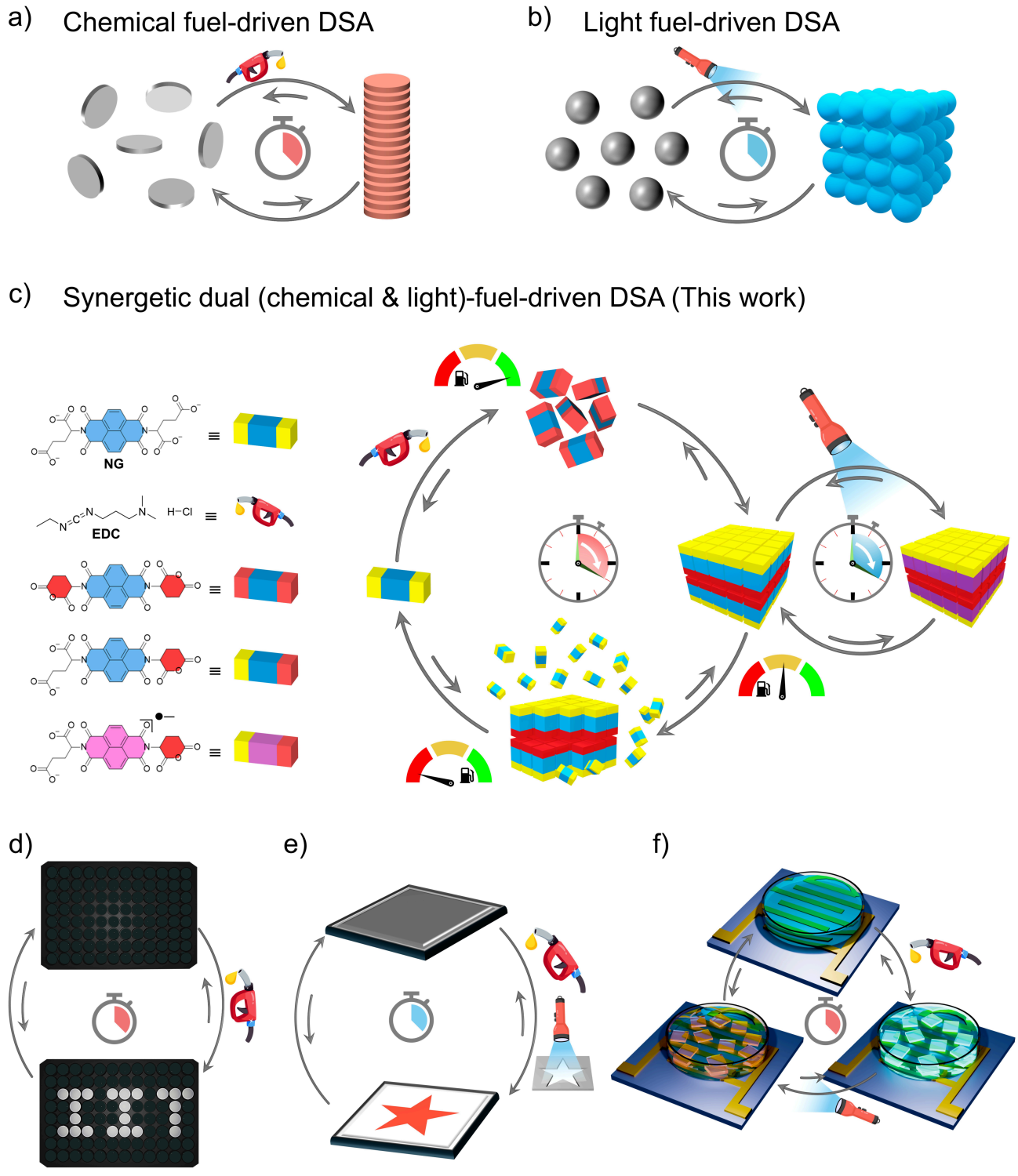


Figure 1

Schematic Overview of the Designed NG Synergistic Dual-Fuel-Driven DSA Process and its Applications. (a-b) Examples of previously reported single-fuel DSA: chemical fuel (a) and light fuel (b). (c) Chemical structures and Illustration of the synergistic dual-fuel-driven DSA process within the developed bioorganic NG molecular system. (d) Chemical fuel-driven self-erasing information writing. (e)

Application of synergistic dual-fuel-driven techniques for spatiotemporal patterning. (f) Development of transient (opto-)electronic devices enabled by the synergistic dual-fuel approach.

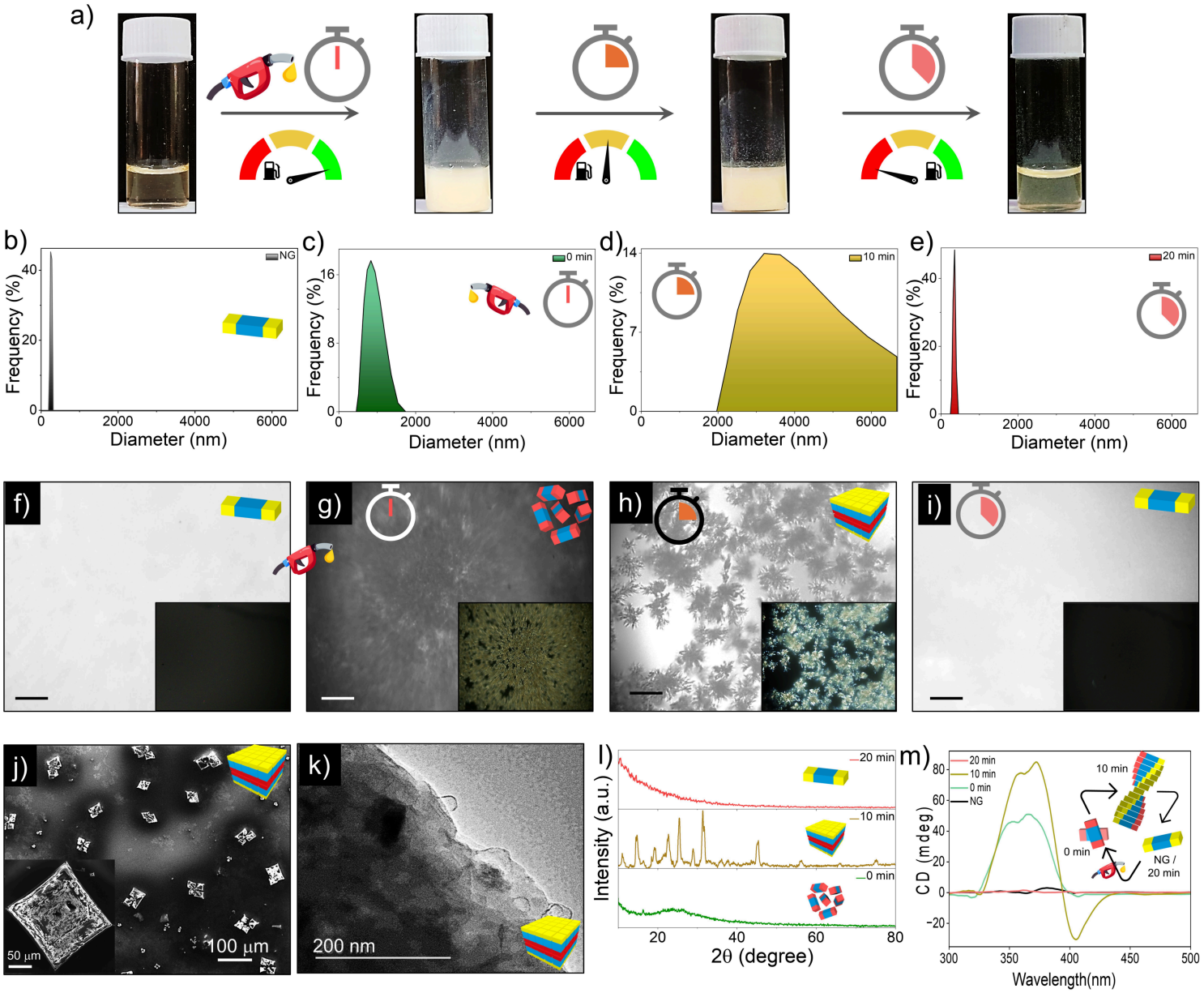


Figure 2

Evolution of Various States of DSA Structures Driven by Chemical Fuel (EDC). (a) Time-resolved photographs demonstrating the EDC-induced visible DSA process in NG. The sequence shows a clear, dissolved pre-fueled solution; a turbid colloidal suspension immediately after fuel addition (0 min); a turbid microcrystalline suspension (10 min post-fuel addition); and a return to a clear solution as the fuel depletes (20 min). (b–e) Time-dependent dynamic light scattering (DLS) size distributions reflecting the changes in self-assembly size during the DSA process: pre-EDC fueled NG (b), and post-EDC fueled NG at 0 min (c), 10 min (d), and 20 min (e). (f–i) Optical microscopy images (with corresponding crossed polarizer images inset) of the pre-EDC fueled NG solution (f), and post-EDC fueled NG at 0 min (g), 10

min (h), and 20 min (i). Scale bars represent 500 μm. (j) High-resolution scanning electron microscopy (HR-SEM) image of the post-EDC fueled NG solution after 10 min, revealing square-shaped 2D crystals. (k) High-resolution transmission electron microscopy (HR-TEM) image displaying the layered hierarchical organization within 2D crystals. (l) X-ray diffraction (XRD) patterns of post-EDC fueled NG self-assemblies at 0 min, 10 min, and 20 min. (m) Circular dichroism (CD) spectral characteristics of pre- and post-EDC fueled NG solutions at 0 min, 10 min, and 20 min, with an inset illustrating the fuel-driven chiral DSA process in NG.

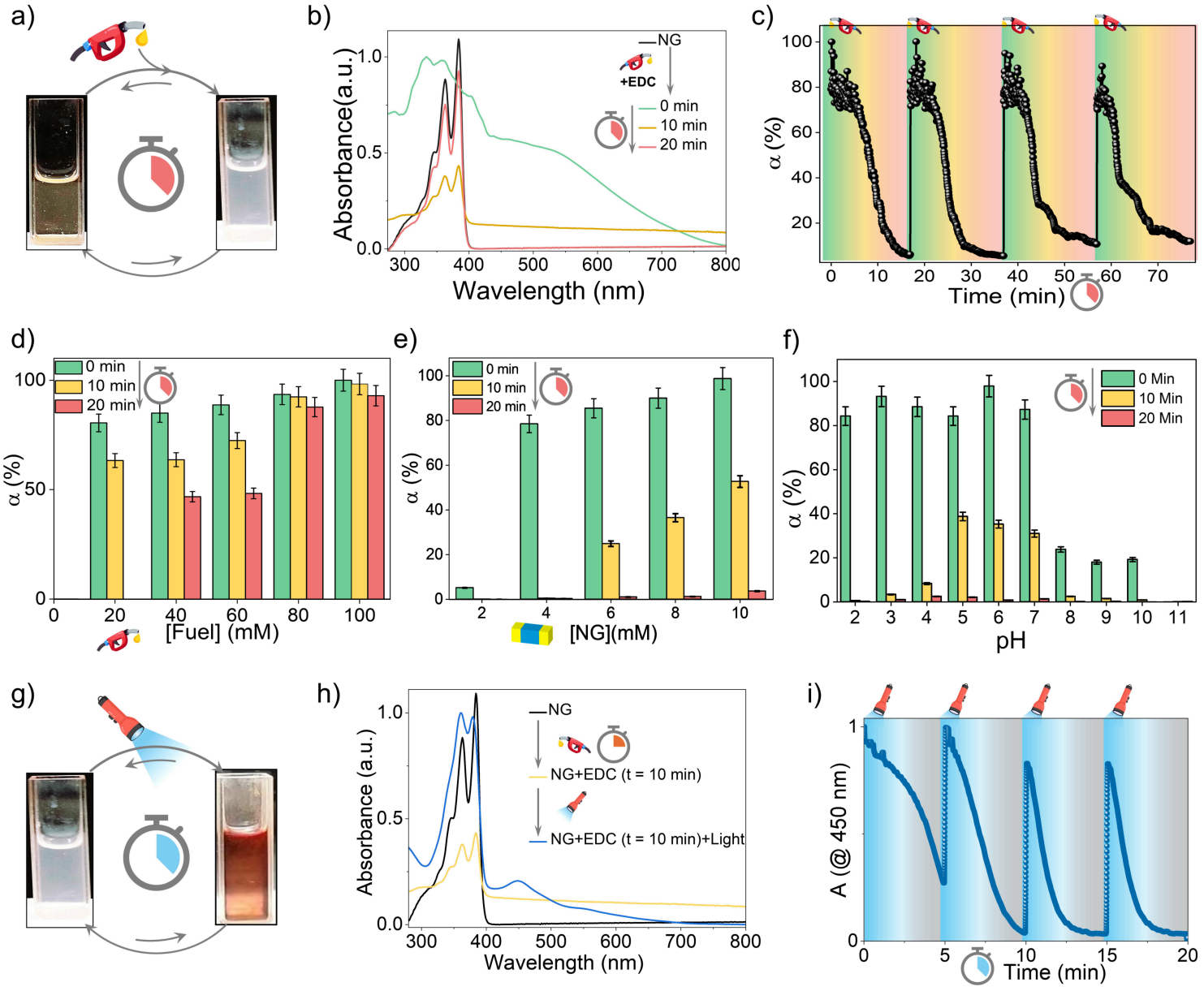


Figure 3

Photophysical Characterization of NG Fuel-Driven DSA Process. (a) Photographs showing the temporal transition of the NG solution from clear to white, turbid phases before and after EDC fueling. (b) UV–vis absorption spectra comparing the NG solution with its post-EDC-fueled solutions at 0, 10, and 20

minutes. (c) The relative percentage of NG aggregation (α%) across consecutive EDC-fueled cycles. (d–f) The temporal relative percentage of post-fueled NG aggregation (α%) (at 0 min, 10 min, and 20 min) plots as a function of fuel (EDC) concentration (d), precursor (NG) concentration (e), and pH of the reaction medium (f). Error bars indicate the mean ± SD (n = 3). (g) Photographs depicting the temporal transformation of the post-EDC-fueled NG solution (10 min) from a white, turbid phase to a deep brown, turbid phase following light exposure. (h) UV–vis absorption spectra of the NG solution after 10 min of EDC-fueled treatment and subsequent light illumination. (i) Temporal normalized absorbance at 450 nm during cycles of light on (blue region) and off (gray region) process.

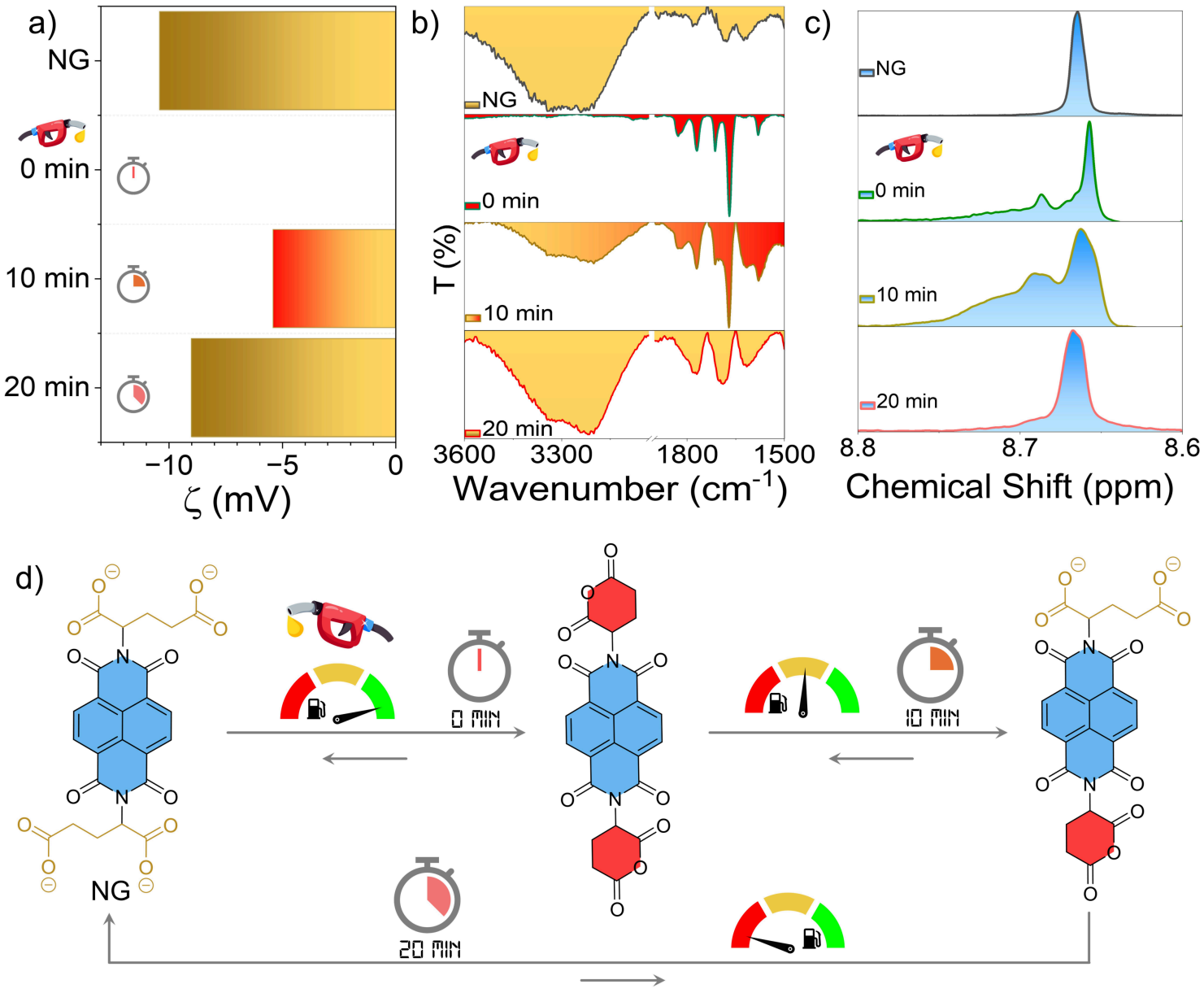


Figure 4

Spectroscopic Analysis of the EDC-Induced Temporal Reaction Cycle in NG. (a) Zeta potential values before and after the introduction of EDC in the NG solutions over time. (b) Selected area time-dependent

changes in FT-IR spectra, comparing pre- and post-EDC NG solutions. (c) Selected areas of time-dependent changes in ^{1}H-NMR spectra, comparing pre- and post-EDC NG solutions. (d) Proposed mechanism illustrating the EDC-driven temporal reaction cycle in NG, as inferred from the spectroscopic data.

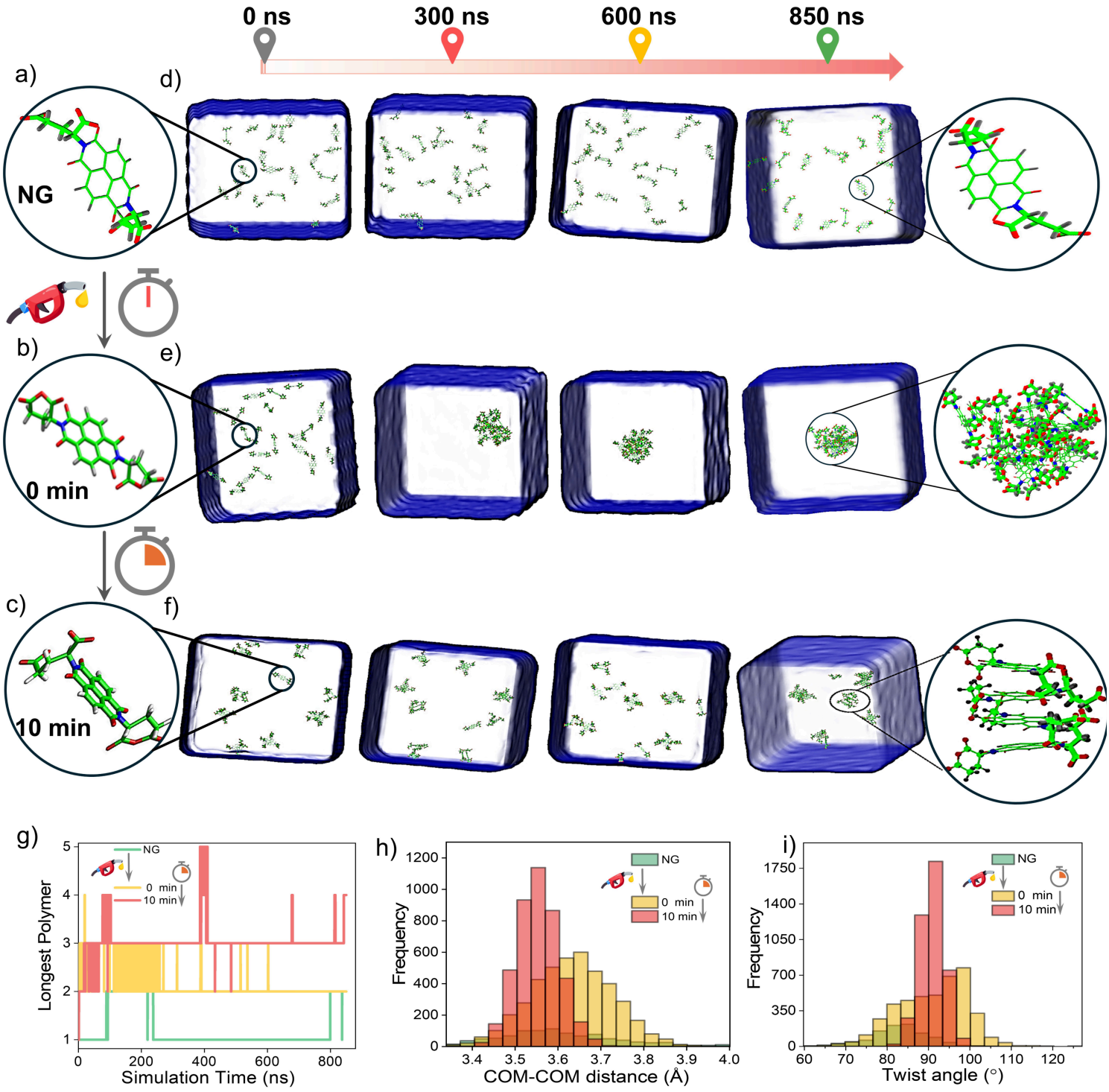


Figure 5

Insights from Atomistic Molecular Dynamics (MD) Simulations on the EDC-Driven DSA Process in NG. (a-c) Molecular structures of NG are shown at three distinct phases: the pre-fuel clear solution state (a), the 0-minute post-fuel white turbid colloidal state (b), and the 10-minute post-fuel microcrystalline state (d) used in the MD simulations. (d-f) The MD snapshots illustrate the self-assembly evolution of NG over time (0, 300, 600, and 850 ns), from the pre-fuel state (d) to the post-fuel states (0 min (e) and 10 min (f)). (g) The temporal evolution of the longest supramolecular polymer length is presented for the three phases. (h) The distribution of center-of-mass (COM) distances between neighboring aromatic cores across the three phases. (i) The distribution of twist angles between adjacent aromatic units at the three phases. All simulations were conducted at 300 K, 1 atm, and pH 7.4. Water molecules have been omitted for clarity. Color coding: carbon (green), nitrogen (blue), oxygen (red), and hydrogen (tan).

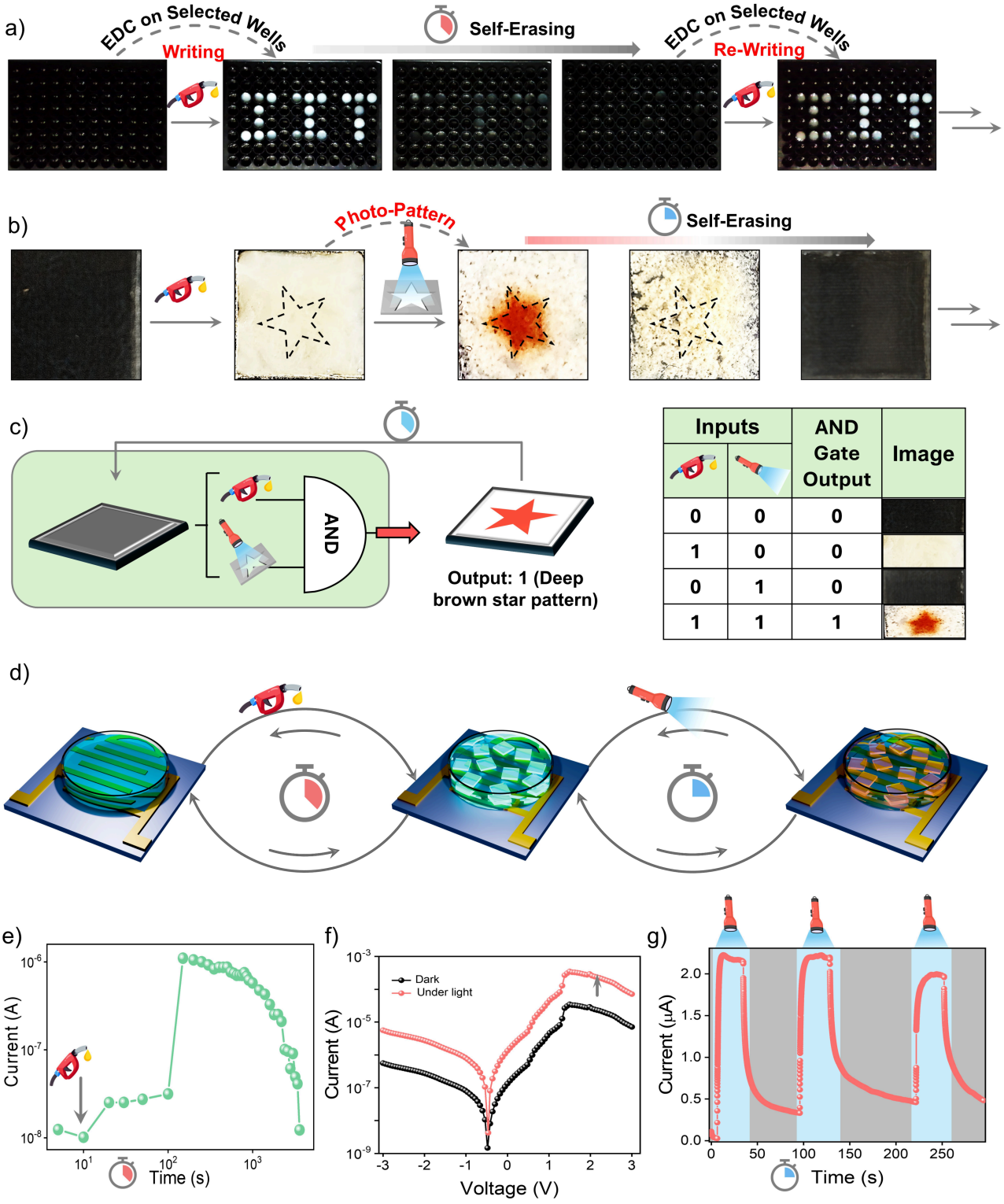


Figure 6

Fuel-Driven Spatiotemporal Multifunctionality Beyond Equilibrium. (a) A self-erasable temporal message "IIT" is created on a 96-well plate filled with NG by spatially applying EDC. (b) Formation of a “star” pattern is driven by the synergistic effects of dual fuels (EDC and light). (c) The schematic illustrates the dual-fuel-driven dissipative systems architecture, which processes inputs from EDC and light using AND logic to yield a specific output: a spatiotemporal “star” pattern resulting from the

combined generation of microcrystals and transient radical anions. A complete truth table derived from these experiments reflects the performance of the double-input AND logic gate. (d) Schematic representation of the device designed to explore the in situ dual fuel-driven (opto-)electronic properties of NG during the DSA process. (e) In situ current (I) measurements are conducted over time during the EDC-driven DSA process in NG. (f) Current (I) versus voltage (V) characteristics of the EDC-driven dissipative crystals are presented under both dark and light conditions. (g) Temporal (opto-)electronic properties of EDC-driven dissipative crystals are shown during cycles of light activation (blue region) and deactivation (gray region).

Supplementary Files

This is a list of supplementary files associated with this preprint. Click to download.

- SIMovieS1.mp4
- SIMovieS2.mp4
- TableofContents.docx